AGU PUBLICATIONS

Geophysical Research Letters

RESEARCH LETTER
10.1002/2016GL070677

Special Section:
First results from NASA's Magnetospheric Multiscale (MMS) Mission

Dipolarization in the inner magnetosphere during a geomagnetic storm on 7 October 2015

H. Matsui[1], P. J. Erickson[2], J. C. Foster[2], R. B. Torbert[1], M. R. Argall[1], B. J. Anderson[3], J. B. Blake[4], I. J. Cohen[3], R. E. Ergun[5], C. J. Farrugia[1], Yu. V. Khotyaintsev[6], H. Korth[3], P.-A. Lindqvist[7], W. Magnes[8], G. T. Marklund[7], B. H. Mauk[3], K. W. Paulson[1], C. T. Russell[9], R. J. Strangeway[9], and D. L. Turner[4]

[1]Space Science Center, University of New Hampshire, Durham, New Hampshire, USA, [2]Haystack Observatory, Massachusetts Institute of Technology, Westford, Massachusetts, USA, [3]The Johns Hopkins University Applied Physics Laboratory, Laurel, Maryland, USA, [4]Space Sciences Department, The Aerospace Corporation, El Segundo, California, USA, [5]Laboratory for Atmospheric and Space Physics, University of Colorado Boulder, Boulder, Colorado, USA, [6]Swedish Institute of Space Physics, Uppsala, Sweden, [7]Royal Institute of Technology, Stockholm, Sweden, [8]Space Research Institute, Austrian Academy of Sciences, Graz, Austria, [9]Institute of Geophysics and Planetary Physics, University of California, Los Angeles, California, USA

Key Points:
- Dipolarization accompanied by tailward convection is interpreted in terms of the pressure balance
- Spatial scales of the irregular part are inferred to be of the order of the ion gyroradius
- Ionospheric measurements place MMS measurements at the poleward edge of the midlatitude trough

Supporting Information:
- Supporting Information S1
- Figure S1
- Figure S2
- Figure S3

Correspondence to:
H. Matsui,
hiroshi.matsui@unh.edu

Citation:
Matsui, H., et al. (2016), Dipolarization in the inner magnetosphere during a geomagnetic storm on 7 October 2015, *Geophys. Res. Lett.*, *43*, 9397–9405, doi:10.1002/2016GL070677.

Received 1 AUG 2016
Accepted 31 AUG 2016
Accepted article online 5 SEP 2016
Published online 19 SEP 2016

Abstract A dipolarization event was observed by the Magnetospheric Multiscale (MMS) spacecraft at $L = 3.8$ and 19.8 magnetic local time starting at ~23:42:36 UT on 7 October 2015. The magnetic and electric fields showed initially coherent variations between the spacecraft. The sunward convection turned tailward after the dipolarization. The observation is interpreted in terms of the pressure balance or the momentum equation. This was followed by a region traversed where the fields were irregular. The scale length was of the order of the ion gyroradius, suggesting the kinetic nature of the fluctuations. Combination of the multi-instrument, multispacecraft data reveals a more detailed picture of the dipolarization event in the inner magnetosphere. Conjunction ionosphere-plasmasphere observations from DMSP, two-dimensional GPS total electron content, the Millstone Hill midlatitude incoherent scatter radar, and AMPERE measurements imply that MMS observations are located on the poleward edge of the ionospheric trough where Region 2 field-aligned currents flow.

1. Introduction

The dipolarization of the geomagnetic field is a common phenomenon during active periods. Early observations were made at or near geosynchrnous orbit [*Cummings et al.*, 1968; *McPherron et al.*, 1973]. The events were measured in a wide spatial range at geosynchronous orbits with different magnetic signatures depending on local time [*Nagai*, 1982]. The azimuthal propagation speed was determined as ~20–30 km/s [*Arnoldy and Moore*, 1983]. It has been reported that there are concurrent energetic particle injections [*Walker et al.*, 1976; *Lopez et al.*, 1988; *Gabrielse et al.*, 2014]. Energetic ions are often seen on the duskside, while electrons are seen on the dawnside [*Thomsen et al.*, 2001]. The dipolarization events are also associated with large electric fields, which were interpreted as inductive [*Aggson et al.*, 1983].

Similar events were also observed in various regions of the magnetosphere. In the magnetotail, bursty bulk flows toward the Earth are often accompanied by dipolarization signatures [*Angelopoulos et al.*, 1992]. This region forms the dipolarization front as revealed by the multispacecraft Cluster mission [*Nakamura et al.*, 2002]. Dipolarization fronts have spatial scales shorter than the ion gyroradius [*Runov et al.*, 2011]. Dipolarization events or injection events have also been observed in the inner magnetosphere inside geosynchronous orbit [*Ohtani et al.*, 2007; *Nosé et al.*, 2010; *Gkioulidou et al.*, 2015; *Turner et al.*, 2015]. The innermost observations of dipolarizations and injections were made as far inside as $L = 3.8$ and 2.5, respectively. In this case, the scale length of the events would be longer than the ion gyroradius so that the physical mechanisms related to the dipolarization are possibly different from those in the magnetotail.

There have been reports that dipolarization events or other active phenomena are accompanied by fluctuations of fields. Pi2 waves were observed together with bursty bulk flows [*Shiokawa et al.*, 1998]. Substorm intensifications and standing waves or field line resonances (FLRs) were found to be associated [*Takahashi et al.*, 1988; *Samson et al.*, 1992; *Rae et al.*, 2014]. FLRs during a dipolarization event may accompany kinetic

scales [*Chaston et al.*, 2014]. Large-amplitude electric fields at the flow braking region has a kinetic or turbulent nature and the Alfvénic Poynting flux can be the energy source for aurora [*Ergun et al.*, 2015].

Substorm signatures were also reported by ground radar measurements [*Foster et al.*, 1981; *Robinson and Vondrak*, 1990; *Sandholt et al.*, 2002; *Grocott et al.*, 2006]. It is possible to derive various quantities including velocity, density, and temperature from incoherent scatter radars. Magnetograms and optical, low-altitude spacecraft, and GPS total electron content (TEC) measurements were often combined to complement the analyses. These measurements could be compared with magnetospheric signatures to provide perspectives on the global magnetosphere-ionosphere (M-I) coupling.

In this study, we report on a dipolarization event measured by the Magnetospheric Multiscale (MMS) mission [*Burch et al.*, 2016] launched in March 2015. Even though the primary goal of the MMS mission is to understand the dynamics of magnetic reconnection, the MMS orbit with a perigee ~1.3 R_E geocentric distance allows high-quality measurements of the inner magnetosphere by some of the instruments including the double probe electric field and energetic particle instruments. The MMS constellation consists of four spacecraft with identical suites of instrumentation. The analysis of multipoint satellite observations [*Paschmann and Daly*, 1998] depends strongly on the spacecraft separation. The objective of this study is to examine a dipolarization event measured in the inner magnetosphere combining the multi-instrument, multispacecraft data. We also report measurements made during the same period by the DMSP satellite constellation, the Millstone Hill incoherent scatter radar, ground-based vertical total electron content (TEC), and the AMPERE measurement for geospace localization of the MMS multipoint observations. This would complement a similar conjunction study within the subauroral polarization stream (SAPS) regions reported by *Erickson et al.* [2016].

2. A Dipolarization Event on 7 October 2015

A dipolarization event was measured by MMS 2 at $L = 3.8$ and 19.8 magnetic local time (MLT) starting at 23:42:36 UT on 7 October 2015. Similar signatures were measured by other MMS spacecraft, although the start time is a little bit shifted by a few seconds. During this event, the spacecraft were operated in the slow survey mode [*Fuselier et al.*, 2016]. Nonetheless, there are a certain amount of data including electromagentic fields [*Torbert et al.*, 2016] and energetic particles [*Mauk et al.*, 2016] available.

There was a geomagnetic storm on 6–8 October 2015. A few peaks of *Dst* values were recorded. The latest decrease started at 13 UT on 7 October. The minimum *Dst* value was −124 nT at 22 UT and the event analyzed occurred just after the *Dst* value started to recover. Concerning the *AU* and *AL* indices, there are slight increases of the activity beginning at ~23:38–23:39 UT. The maximum and minimum values for each index were 183 and −208 nT, respectively. (The maximum *AE* value was 349 nT.) At this time, the *Kp* index was 6, indicating that the Alfvén layer contracted close to the Earth. We have selected this event because the observation was made well inside the inner magnetosphere, at a location being in a magnetic conjunction with the Millstone Hill radar.

Figure 1 shows an overview plot for an interval 23:35–23:50 UT including this event. At this time, the spacecraft was moving toward the perigee, as measured by the fluxgate magnetometers [*Russell et al.*, 2016]. The number density derived from the spacecraft potential [e.g., *Pedersen et al.*, 2008] does not decrease much during this event, implying that the measurements were not made in the lobe. Around this interval, the spacecraft was located in the ring current region as identified by enhanced energetic ions measured by Fly's Eye Energetic Particle Spectrometer (FEEPS) [*Blake et al.*, 2016] and electrons from Energetic Ion Spectrometer [*Mauk et al.*, 2016]. Note that all data except the ion flux come from MMS 2 in this figure. Concerning the ion flux, spin-averaged data from all spacecraft are combined for both the top and bottom detectors ID 6 on FEEPS, in order to increase the time resolution. In return, there is an artificial tone every ~200 s, visible in the fourth panel.

A dipolarization event was identified, at the time of the vertical line, by the sudden increase of the northward magnetic field B_H, being faster than that of the background geomagnetic field. By MMS 2 the event was observed with the following sequence: start decreasing B_H(= 331 nT) at 23:41:38, minimum of B_T(= 572 nT) at 23:42:12, minimum of B_H(= 309 nT) or start of the dipolarization at 23:42:36, and maximum of B_H(= 450 nT) at 23:46:11. Note that the magnetic elevation angle increases from 31.7 to 42.5° coincident with that of B_H (Figure S1 in the supporting information). This is about twice the increase rate of the background elevation angle. The dipolarization event is associated with variations of electric fields with amplitudes > 20 mV/m

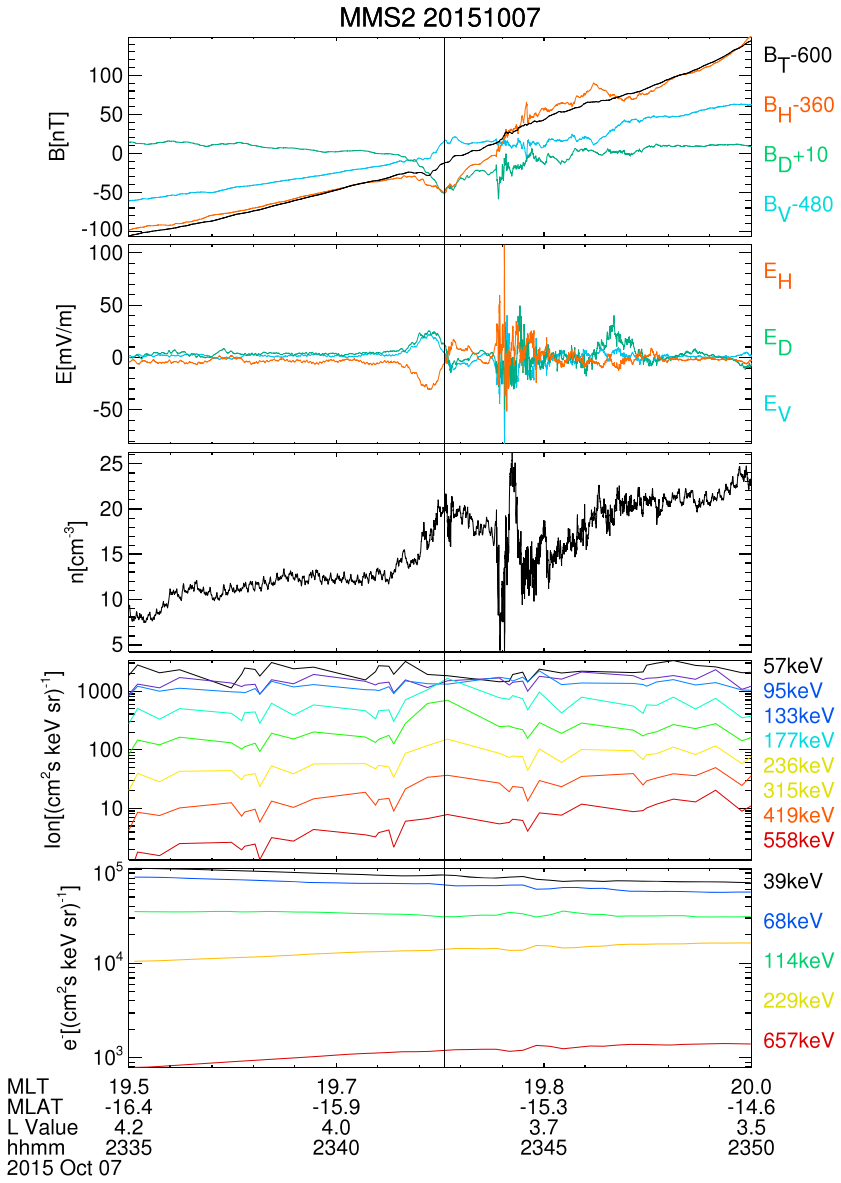

Figure 1. MMS measurements on 23:35–23:50 UT, 7 October 2015. The following quantities are plotted from top: magnetic fields, electric fields, number density derived from the spacecraft potential, energetic ion flux, and energetic electron flux. Each component of the fields is plotted in cylindrical, VDH coordinates: outward, eastward, and northward components. Ephemeris information is shown in the bottom. All data except energetic ions are from MMS 2. Energetic ion data are a combination from all spacecraft. A dipolarization event started at the time of the vertical line.

(> 80 mV/m at maximum) as measured by the double probes [*Lindqvist et al.*, 2016; *Ergun et al.*, 2016]. The earlier part at 23:41:30–23:43:30 UT consists of rather laminar, smooth variations, while the later part at 23:43:30–23:46:30 UT is irregular with large amplitudes of fluctuations. It is possible to infer that there are two such parts from previous observations [e.g., *Gkioulidou et al.*, 2015]. Nonetheless, this signature has not drawn attention from the viewpoint of electric field data analysis or multiple spacecraft data analysis with close separation. After the B_H component starts to decrease, the E_V component becomes positive, indicating a sunward convection. There is a peak of the E_V component during the decrease of the B_H component. Then, the B_H value starts to increase, that is, the dipolarization starts when the sign of the E_V component turns to negative. After that, the electric and magnetic fields show oscillating features with a mix of both longer periods of minutes and shorter periods of seconds.

There is a density increase accompanied by the B_H decrease. A peak of the density is identified around the time when the dipolarization starts. The ion flux increases at the energies ~150–400 keV concurrent with that of the density, whereas the flux at the lower energies ~60–120 keV rather decreases. The electron counts only show slight variations. This implies that the spacecraft are on the duskside flank of the dipolarization from boundary in MLT [*Gabrielse et al.*, 2014]. The mismatch of magnetic field and particle flux changes is different from the typical dipolarization and injection in the tail, where both quantities increase at the same time and are explained in terms of the conservation of particles' first adiabatic invariant. Note that there is another difference from the tail that the scale length of the dipolarization in the inner magnetosphere is longer than the ion gyroradius because of the large background magnetic field for one reason. In our case, the gyroradius is estimated as 110 km, where we use the energy of peak flux at 180 keV since we do not have plasma moment values. The scale length of the dipolarization event will be discussed below.

Next we explain the interspacecraft configuration around this event at 23:41 UT (Figure S2), which is useful for the analyses below. The spacecraft separations were 20–120 km at this time. The shape was not tetrahedral because of the orbit close to the perigee, which is not the primary survey area for MMS. The spacecraft were coplanar as inferred from the d*Y*-d*Z* plane projection, although the constellation was not a pearl-on-a-string shape either. Therefore, the current density from the curlometer technique [*Dunlop et al.*, 1988] may be estimated for one component. Each line in the figure indicates the spacecraft motion for 30 s, implying that a temporal variation on the order of this period may be separated from a spatial variation.

3. Initial Part With Smooth Variations

We analyze the initial part with the smooth variations in more detail. Figure 2 (left column) shows an interval including such magnetic and electric field variations from all spacecraft in field-aligned coordinates, in which each component corresponds to the one parallel to the magnetic field (suffix ||), the perpendicular and radial one (perp,R or $\perp R$), and the perpendicular and azimuthal one (perp,A or $\perp A$). Data are high-pass filtered at a period of 600 s. This figure shows that the magnetic and electric field variations were coherent between spacecraft. Below we perform more detailed analyses of these data.

Concerning the propagation of the structure, the convection velocity is first westward and then turns to eastward. The maximum speed is 50 km/s, when we refer to the amplitude of the radial electric field 30 mV/m and the background geomagnetic field 580 nT. This speed is comparable to the typical gradient B drift speed of energetic ions of 30 km/s. Here we used the values $L = 3.9$ and the particle energy 180 keV based on the measurement. Dipole geomagnetic field was assumed. We cannot get a reliable speed from the timing method using the multispacecraft data presumably because the spacecraft separation is small compared to the scale size of the event. This is demonstrated by the timing difference on the order of 1 s and the magnetic field variation on the order of 60–120 s.

Next we compare electric field variations and magnetic field variations. The phase difference between magnetic and electric fields is ~90°, similar to the inductive field previously inferred [*Aggson et al.*, 1983; *Ohtani et al.*, 2007]. This situation is also similar for standing waves. The primary direction of the variations is azimuthal for the magnetic field and radial for the electric field, indicating toroidal. If we assume that the measured fluctuation is due to propagating waves, the phase velocity is estimated as ~ 750 km/s. Here we use the measured peak amplitude of the azimuthal fluctuation as 40 nT and the wave period as 60 s. The Alfvén velocity at this time is ~3000 km/s, based on the number density 17 cm^{-3} and assuming single species of protons. The calculated Alfvén velocity is larger than the phase velocity possibly because of the standing waves and/or the presence of heavy ions.

We may estimate the current density for this event from the following three methods: (1) assuming a spatial structure with some shape, (2) the curlometer technique, and (3) assuming Alfvénic fluctuations. Two components of the current density, $J_{\parallel}$ and $J_{\perp R}$, are calculated below. Assuming a spatial structure, these two components may be estimated as $J_{\parallel} = -17$ nA/m^2 and $J_{\perp R} = -4$ to -3 nA/m^2. The radial magnetic fluctuation 40 nT, the parallel fluctuation 10 nT, and the distance 1 R_E from the equator are introduced. The azimuthal scale is assumed as ~ 0.3 R_E from the particle motion with 30 km/s for 60 s. We do not introduce the radial gradient term estimated from the spacecraft motion mainly in the radial direction because the calculated value is not consistent with that from the curlometer technique below. Therefore, the measured variation is likely to not be spatial but rather temporal. In addition, the two terms contributing to $J_{\perp R}$, the gradient term of the parallel magnetic fluctuations and that of azimuthal fluctuations, are not added because the peak of each

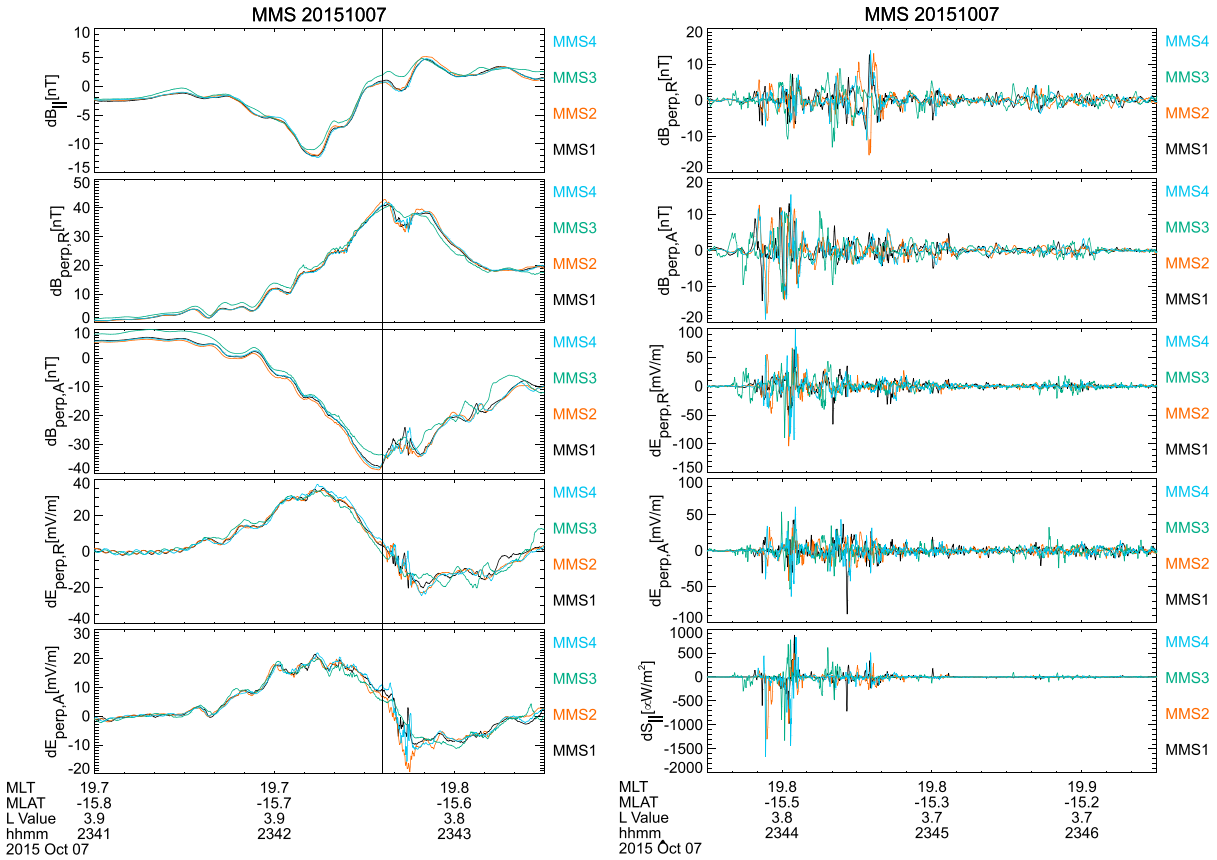

Figure 2. (left column) Magnetic and electric field variations between 23:41:00 and 23:43:30. Data from all spacecraft are high-pass filtered at a period of 600 s and shown in the field-aligned coordinates. A dipolarization event started at the time of the vertical line. See text for the detail. (right column) Magnetic and electric field variations and Poynting flux between 23:43:30 and 23:46:30. Data are high-pass filtered at a period of 10 s.

value is shifted in time. Using the curlometer technique, $J_{\parallel}$ is ~-50 nA/m^2. Note that the direction of the current or the normal of the spacecraft constellation chosen (MMS 2–4) is rather antiparallel to the magnetic field (~140°). The sign of the calculated value is consistent with that assuming a spatial structure as noted above. The direction is pointing toward the ionosphere, the same sense as the Region 2 current, and is consistent with the precipitation of injected ions. Concerning the method assuming propagating Alfvénic fluctuations, $J_{\perp R}$ is estimated as 4 nA/m^2, leaving the freedom of the sign, and is similar to the values assuming a spatial structure. However, the actual fluctuation would be standing as inferred above so that the calculated $J_{\perp R}$ here only indicates an order of magnitude.

Next we evaluate the pressure balance in the azimuthal direction or the corresponding momentum equation during our measurement. The $J \times B$ term may be written as follows: $J \times B = \nabla(B^2/2\mu_0) + (B \cdot \nabla)(B/\mu_0)$, where μ_0 is the permeability in vacuum. The first term on the right side is related to the magnetic gradient, while the second term is the magnetic tension force. These terms are estimated as $2.4 \cdot 10^{-15}$ J/m^2 and $1.6 \cdot 10^{-15}$ J/m^2, respectively. Note that the peak of each term is shifted in time, the same as the calculation of $J_{\perp R}$, so that these two values may not be accumulated. These values are comparable to the pressure gradient term $2.3 \cdot 10^{-15}$ J/m^2 assuming 0.15 cm^{-3} of 180 keV protons with a spatial scale of 0.3 R_E. There is a constraint on the comparison performed here. Measured density and temperature, and hence thermal pressure, should be derived from plasma moment calculations. However, the plasma moments are not available for this event, as mentioned before, so that the above density and temperature of the energetic protons have been assumed. An additional term in the momentum equation is the inertial term $mn(\mathrm{d}v/\mathrm{d}t)$, which is calculated to be $-5 \cdot 10^{-17}$ J/m^2, assuming a time scale of 30 s, single species of protons, and neglecting the spatial gradient term. The calculated inertial term is much smaller than the $J \times B$ term and possibly the ∇p term as well and may be neglected.

Therefore, we may interpret our measurement as follows. The magnetic field lines are stretched due to the energetic particle motions, its gradient, and the relevant stress balance. The motion of the magnetic field lines leads to the enhanced electric field. At some point, the magnetic tension force is larger than the pressure gradient force so that the field lines move back. Then the field lines may move back and forth due to the inertial motion as ultralow frequency oscillations. The standing waves or FLRs during substorms have been previously reported [*Takahashi et al.*, 1988; *Samson et al.*, 1992; *Rae et al.*, 2014]. This would explain a measurement which is different from that typical in the magnetotail: After starting the dipolarization, the direction of convection is eastward or tailward.

4. Later Part With Irregular Variations

Next we examine the later part of this event. Figure 2 (right column) shows two perpendicular components of electric fields and magnetic fields and a parallel component of the Poynting flux. The data are high-pass filtered at 10 s. The electromagnetic fields became irregular unlike the initial part. When we calculate correlations with shifted time lags between each pair of the spacecraft for our data with 8 Hz sampling, the spatial scales may be estimated as ~45 km for the magnetic fields and ~25 km for the electric fields. These scales are determined as the distances by which the correlation coefficient reduces to ~0.4. It is possible that particles precipitate into the ionosphere due to these fluctuations. This is because the fluctuations are irregular so that they have a kinetic scale. In our case, the ion gyroradius is of the order of ~110 km. Kinetic Alfvén waves accompany parallel electric fields [e.g., *Chaston et al.*, 2014]. Concerning the parallel Poynting flux, the direction tends to point toward the ionosphere in the same hemisphere as the spacecraft. The size of the Poynting flux ~1 mW/m^2 at maximum is similar to that reported by *Ergun et al.* [2015].

5. Geospace Localization of MMS Observations

Simultaneous observations of the ionosphere and plasmasphere by ground-based and low-altitude plasma sensors were available during the time MMS observed the dipolarization event and associated current structures in Figure 2. In particular, the Millstone Hill incoherent scatter radar [*Foster and Vo*, 2002; *Erickson et al.*, 2011] has a wide field of view spanning subauroral and auroral latitudes and was operated to provide magnetically conjugate measurements of plasma conditions during the southbound MMS pass. Ground-based determination of two-dimensional vertical total electron content (TEC) from the GPS satellite cluster was also calculated by MIT Haystack Observatory [*Rideout and Coster*, 2006], measuring electron density to ~4 Re. Electron precipitation data delineating Region 1 auroral boundaries were measured by particle instruments on the DMSP spacecraft transiting the topside ionosphere at ~840 km [*Strom and Iwanaga*, 2005].

Figure 3 (top) shows GPS total electron content measurements on a 1° by 1° geodetic latitude/longitude grid with 20 min temporal averaging at 23:40 UTC. The thick magenta line marks the equatorward extent of electron precipitation from near-simultaneous observations by DMSP F17A and F19 satellites passing through the same longitude sector at 23:53 UTC. The thick red line marks the MMS magnetic footprint based on the Tsyganenko model [*Tsyganenko and Sitnov*, 2005] during the times of significant magnetic and electric field variations in Figure 2. Figure 3 (bottom) plots Millstone Hill radar determined electron density at 400 km altitude for two different radar scan times, binned in ~0.5° increments on average as a function of invariant latitude. Uncertainties on electron density are 5-10% (not shown for clarity). The shaded grey region indicates the magnetically mapped MMS footprint of Figure 2, while the dashed line marks the 23:53 UTC DMSP equatorward electron precipitation boundary.

The Millstone Hill electron density and GPS TEC observations clearly show the establishment of a stable mid-latitude electron density trough at the time of MMS transit, and DMSP precipitation boundaries localize the significant MMS in situ fluctuations as being subauroral but on the poleward edge of the trough. These signatures are consistent with previous studies showing that the major downward Region 2 field-aligned current region is at the poleward edge of the trough [*Nilsson et al.*, 2005] and also agree well with MMS indications that injected species are primarily ions with lack of enhanced electron precipitation. Although not shown, Millstone Hill radar data at ~22:30 UTC also show a well-defined and strong velocity signature over several degrees latitude characteristic of a subauroral polarization stream electric field (SAPS) [*Foster and Burke*, 2002; *Erickson et al.*, 2011], extending to 57° invariant latitude. The presence of significant SAPS poleward fields in this longitude sector are a strong indication of the importance of large-scale M-I coupling during the dipolarization event.

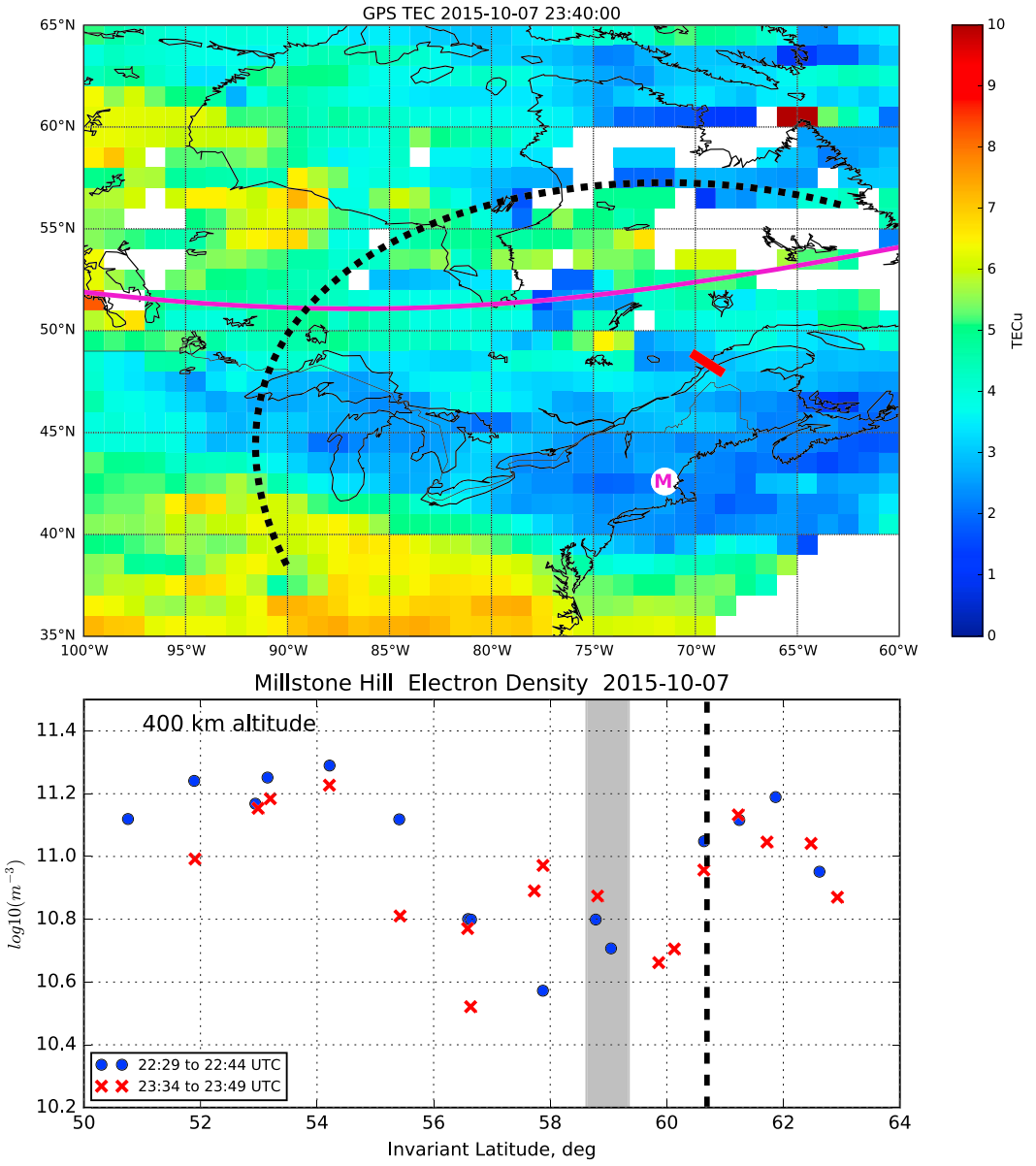

Figure 3. (top) GPS vertical total electron content map (1° by 1° by 20 min averaging) at 23:40 UTC, with MMS track (thick red line; the time period in Figure 2). The thick magenta line marks the equatorward electron precipitation boundary from simultaneous DMSP F17A and F19 passes. Millstone Hill radar coverage of ionospheric parameters at 400 km altitude is shown with the thick dotted black line. (bottom) Millstone Hill incoherent scatter radar observations of electron density at 400 km altitude at two indicated radar scan times, binned in ~0.5° invariant latitude steps on average. The shaded grey region is the MMS magnetic footprint of Figure 2, while the dashed line is the DMSP electron precipitation boundary. Observations localize MMS measurements in Region 2 FAC areas at the poleward edge of a stable midlatitude trough.

We also have conjunction AMPERE measurements made by one of Iridium satellites located at ~0.4 h MLT westward of MMS [*Anderson et al.*, 2000] (Figure S3). The eastward magnetic deviations of AMPERE decrease with decreasing latitudes after ~23:44 UT, indicating measurements of the Region 2 current. The poleward edge of the current is identified as ~57.5–59.7° of invariant latitudes, a range within horizontal bars, and is comparable to the invariant latitudes of the MMS magnetic footprint in Figure 3 (bottom). This supports the above description of ionospheric localization of MMS measurements, taking into account that the location of the trough depends on altitudes and MLT.

6. Summary

A dipolarization event was measured by MMS in the inner magnetosphere at $L = 3.8$ and 19.8 MLT at ~23:42:36 UT, 7 October 2015, accompanied by an injection of energetic ions. Electrons show only slight variations. The event consists of two parts: the initial laminar part and the later irregular part. During the initial part, the magnetic and electric fields show mostly similar variations between multiple spacecraft. The fluctuations are similar to the toroidal standing waves. The current density estimated may be interpreted in terms of those of the pressure balance or the momentum equation. A possibility is that the $J \times B$ and ∇p terms are balanced. During the later part, the fields are rather irregular. The scale length would be comparable to the spacecraft separation 20–120 km. According to the ionospheric observations, the foot point of MMS corresponds to the poleward edge of the trough where the downward Region 2 current is expected. The Region 2 current measured by AMPERE supports this view. These observations may be consistent with the absence of enhanced energetic electrons. The above analyses imply the importance of multi-instrument, multipoint measurements of dipolarization events. The obtained results provide a detailed feature of a particular dipolarization event and simultaneously a global context through the comparison with ionospheric measurements. In the future, we would like to collect more dipolarization events and to examine whether the event reported here is common. A detailed analysis of the irregular fluctuations to clarify their physical mechanisms is also envisaged.

Acknowledgments
This work was supported by NASA's MMS contract NNG04EB99C. MMS data are publicly available at https://lasp.colorado.edu/mms/sdc/public/. Millstone Hill radar observations and GPS TEC analysis at MIT Haystack Observatory are supported by Millstone Hill Geospace Facility activities under cooperative agreement AGS-1242204 between the National Science Foundation and the Massachusetts Institute of Technology. DMSP satellite data were kindly provided by Kevin Martin and Pat Doherty at Boston College. AMPERE data are available at http://ampere.jhuapl.edu or upon request to the PI (Brian Anderson). Geomagnetic indices were obtained at World Data Center, Kyoto University (http://wdc.kugi.kyoto-u.ac.jp).

References

Aggson, T. L., J. P. Heppner, and N. C. Maynard (1983), Observations of large magnetospheric electric fields during the onset phase of a substorm, *J. Geophys. Res.*, *88*, 3981–3990.
Anderson, B. J., K. Takahashi, and B. A. Toth (2000), Sensing global Birkeland currents with Iridium engineering magnetometer data, *Geophys. Res. Lett.*, *27*, 4045–4048.
Angelopoulos, V., W. Baumjohann, C. F. Kennel, F. V. Coroniti, M. G. Kivelson, R. Pellat, R. J. Walker, H. Lühr, and G. Paschmann (1992), Bursty bulk flows in the central plasma sheet, *J. Geophys. Res.*, *97*, 4027–4039.
Arnoldy, R. L., and T. E. Moore (1983), Longitudinal structure of substorm injections at synchronous orbit, *J. Geophys. Res.*, *88*, 6213–6220.
Blake, J. B., et al. (2016), The Fly's Eye Energetic Particle Spectrometer (FEEPS) sensors for the magnetospheric multiscale (MMS) mission, *Space Sci. Rev.*, *199*, 309–329, doi:10.1007/s11214-015-0163-x.
Burch, J. L., T. E. Moore, R. B. Torbert, and B. L. Giles (2016), Magnetospheric multiscale overview and science objectives, *Space Sci. Rev.*, *199*, 5–21, doi:10.1007/s11214-015-0164-9.
Chaston, C. C., et al. (2014), Observations of kinetic scale field line resonances, *Geophys. Res. Lett.*, *41*, 209–215, doi:10.1002/2013GL058507.
Cummings, W. D., J. N. Barfield, and P. J. Coleman Jr. (1968), Magnetospheric substorms observed at the synchronous orbit, *J. Geophys. Res.*, *73*, 6687–6698.
Dunlop, M. W., D. J. Southwood, K.-H. Glassmeier, and F. M. Neubauer (1988), Analysis of multipoint magnetometer data, *Adv. Space Res.*, *8*(9), 273–277.
Ergun, R. E., K. A. Goodrich, J. E. Stawarz, L. Andersson, and V. Angelopoulos (2015), Large-amplitude electric fields associated with bursty bulk flow braking in the Earth's plasma sheet, *J. Geophys. Res. Space Physics*, *120*, 1832–1844, doi:10.1002/2014JA021065.
Ergun, R. E., et al. (2016), The axial double probe and fields signal processing for the MMS mission, *Space Sci. Rev.*, *199*, 167–188, doi:10.1007/s11214-014-0115-x.
Erickson, P. J., F. Beroz, and M. Z. Miskin (2011), Statistical characterization of the American sector subauroral polarization stream using incoherent scatter radar, *J. Geophys. Res.*, *116*, A00J21, doi:10.1029/2010JA015738.
Erickson, P. J., et al. (2016), Multipoint MMS observations of fine-scale SAPS structure in the inner magnetosphere, *Geophys. Res. Lett.*, *43*, 7294–7300, doi:10.1002/2016GL069174.
Foster, J. C., and W. J. Burke (2002), SAPS: A new characterization for sub-auroral electric fields, *Eos Trans. AGU*, *83*, 393–394.
Foster, J. C., and H. B. Vo (2002), Average characteristics and activity dependence of the subauroral polarization stream, *J. Geophys. Res.*, *107*(A12), 1475, doi:10.1029/2002JA009409.
Foster, J. C., J. R. Doupnik, and G. S. Stiles (1981), Ionospheric convection and currents in the midnight sector on November 8, 1979, *J. Geophys. Res.*, *86*, 2143–2148.
Fuselier, S. A., W. S. Lewis, C. Schiff, J. L. Burch, S. M. Petrinec, and K. J. Trattner (2016), Magnetospheric multiscale science mission profile and operations, *Space Sci. Rev.*, *199*, 77–103, doi:10.1007/s11214-014-0087-x.
Gabrielse, C., V. Angelopoulos, A. Runov, and D. L. Turner (2014), Statistical characteristics of particle injections throughout the equatorial magnetotail, *J. Geophys. Res. Space Physics*, *119*, 2512–2535, doi:10.1002/2013JA019638.
Gkioulidou, M., et al. (2015), Spatial structure and temporal evolution of energetic particle injections in the inner magnetosphere during the 14 July 2013 substorm event, *J. Geophys. Res. Space Physics*, *120*, 1924–1938, doi:10.1002/2014JA020872.
Grocott, A., M. Lester, M. L. Parkinson, T. K. Yeoman, P. L. Dyson, J. C. Devlin, and H. U. Frey (2006), Towards a synthesis of substorm electrodynamics: HF radar and auroral observations, *Ann. Geophys.*, *24*, 3365–3381.
Lindqvist, P.-A., et al. (2016), The spin-plane double probe electric field instrument for MMS, *Space Sci. Rev.*, *199*, 137–165, doi:10.1007/s11214-014-0116-9.
Lopez, R. E., A. T. Y. Lui, D. G. Sibeck, R. W. McEntire, L. J. Zanetti, T. A. Potemra, and S. M. Krimigis (1988), The longitudinal and radial distribution of magnetic reconfiguration in the near-Earth magnetotail as observed by AMPTE/CCE, *J. Geophys. Res.*, *93*, 997–101.
Mauk, B. H., et al. (2016), The energetic particle detector (EPD) investigation and the energetic ion spectrometer (EIS) for the magnetospheric multiscale (MMS) mission, *Space Sci. Rev.*, *199*, 471–514, doi:10.1007/s11214-014-0055-5.
McPherron, R. L., C. T. Russell, and M. P. Aubry (1973), Satellite studies of magnetospheric substorms on August 15, 1968 9. Phenomenological model for substorms, *J. Geophys. Res.*, *78*, 3131–3149.
Nagai, T. (1982), Observed magnetic substorm signatures at synchronous altitude, *J. Geophys. Res.*, *87*, 4405–4417.

Nakamura, R., et al. (2002), Motion of the dipolarization front during a flow burst event observed by Cluster, *Geophys. Res. Lett.*, *29*(20), 1942, doi:10.1029/2002GL015763.
Nilsson, H., T. I. Sergienko, Y. Ebihara, and M. Yamauchi (2005), Quiet-time mid-latitude trough: Influence of convection, field-aligned currents and proton precipitation, *Ann. Geophys.*, *23*, 3277–3288.
Nosé, M., H. Koshiishi, H. Matsumoto, P. C:son Brandt, K. Keika, K. Koga, T. Goka, and T. Obara (2010), Magnetic field dipolarization in the deep inner magnetosphere and its role in development of O^+-rich ring current, *J. Geophys. Res.*, *115*, A00J03, doi:10.1029/2010JA015321.
Ohtani, S., et al. (2007), Cluster observations in the inner magnetosphere during the 18 April 2002 sawtooth event: Dipolarization and injection at $r = 4.6\ R_E$, *J. Geophys. Res.*, *112*, A08213, doi:10.1029/2007JA012357.
Paschmann, G., and P. W. Daly (Eds.) (1998), *Analysis Methods for Multi-Spacecraft Data*, 491 pp., ESA Publications Division, Noordwijk, Neth.
Pedersen, A., et al. (2008), Electron density estimations derived from spacecraft potential measurements on Cluster in tenuous plasma regions, *J. Geophys. Res.*, *113*, A07S33, doi:10.1029/2007JA012636.
Rae, I. J., K. R. Murphy, C. E. J. Watt, G. Rostoker, R. Rankin, I. R. Mann, C. R. Hodgson, H. U. Frey, A. W. Dageling, and C. Forsyth (2014), Field line resonances as a trigger and a tracer for substorm onset, *J. Geophys. Res. Space Physics*, *119*, 5343–5363, doi:10.1002/2013JA018889.
Rideout, W., and A. Coster (2006), Automated GPS processing for global total electron content data, *GPS Solutions*, *10*, 219–228.
Robinson, R. M., and R. R. Vondrak (1990), Electrodynamic properties of auroral surges, *J. Geophys. Res.*, *95*, 7819–7832.
Runov, A., V. Angelopoulos, X.-Z. Zhou, X.-J. Zhang, S. Li, F. Plaschke, and J. Bonnell (2011), A THEMIS multicase study of dipolarization fronts in the magnetotail plasma sheet, *J. Geophys. Res.*, *116*, A05216, doi:10.1029/2010JA016316.
Russell, C. T., et al. (2016), The magnetospheric multiscale magnetometers, *Space Sci. Rev.*, *199*, 189–256, doi:10.1007/s11214-014-0057-3.
Samson, J. C., D. D. Wallis, T. J. Hughes, F. Creuzberg, J. M. Ruohoniemi, and R. A. Greenwald (1992), Substorm intensifications and field line resonances in the nightside magnetosphere, *J. Geophys. Res.*, *97*, 8495–8518.
Sandholt, P. E., C. J. Farrugia, M. Lester, S. Cowley, S. Milan, W. F. Denig, B. Lybekk, E. Trondsen, and V. Vorobjev (2002), Multistage substorm expansion: Auroral dynamics in relation to plasma sheet particle injection, precipitation, and plasma convection, *J. Geophys. Res.*, *107*(A11), 1342, doi:10.1029/2001JA900116.
Shiokawa, K., et al. (1998), High-speed ion flow, substorm current wedge, and multiple Pi 2 pulsations, *J. Geophys. Res.*, *103*, 4491–4507.
Strom, S. R., and G. Iwanaga (2005), Overview and history of the defense meteorological satellite program, crosslink, *Aerosp. Corp. Mag. Adv. Aerosp. Technol.*, *6*(1), 11–15.
Takahashi, K., S. Kokubun, T. Sakurai, R. W. McEntire, T. A. Potemra, and R. E. Lopez (1988), AMPTE/CCE observations of substorm-associated standing Alfvén waves in the midnight sector, *Geophys. Res. Lett.*, *15*, 1287–1290.
Thomsen, M. F., J. Birn, J. E. Borovsky, K. Morzinski, D. J. McComas, and G. D. Reeves (2001), Two-satellite observations of substorm injections at geosynchronous orbit, *J. Geophys. Res.*, *106*, 8405–8416.
Torbert, R. B., et al. (2016), The FIELDS instrument suite on MMS: Scientific objectives, measurements, and data products, *Space Sci. Rev.*, *199*, 105–135, doi:10.1007/s11214-014-0109-8.
Tsyganenko, N. A., and M. I. Sitnov (2005), Modeling the dynamics of the inner magnetosphere during strong geomagnetic storms, *J. Geophys. Res.*, *110*, A03208, doi:10.1029/2004JA010798.
Turner, D. L., et al. (2015), Energetic electron injections deep into the inner magnetosphere associated with substorm activity, *Geophys. Res. Lett.*, *42*, 2079–2087.
Walker, R. J., K. N. Erickson, R. L. Swanson, and J. R. Winckler (1976), Substorm-associated particle boundary motion at synchronous orbit, *J. Geophys. Res.*, *81*, 5541–5550.